Diffraction-limited, 10-W, 5-ns, 100-kHz, all-fiber laser at 1.55 μm

I. Pavlov,[1,*] E. Dülgergil,[2] E. Ilbey,[1] and F. Ö. Ilday[1,3]

[1]*Department of Physics, Bilkent University, 06800 Ankara, Turkey*

[2]*Meteksan Savunma Inc., Ankara, Turkey*

[3]*Department of Electrical and Electronics Engineering, Bilkent University, 06800 Ankara, Turkey*

**Corresponding author: pavlov@fen.bilkent.edu.tr*

Received December 30, 2013; revised March 25, 2014; accepted March 25, 2014; posted March 26, 2014 (Doc. ID 203874); published April 25, 2014

This Letter reports on an all-fiber-integrated master-oscillator, power amplifier system at 1.55 μm producing 5-ns, 100-μJ pulses. These pulses are generated at a 100 kHz repetition rate, corresponding to 10 W of average power. The seed source is a low-power, current-modulated, single-frequency, distributed feedback semiconductor laser. System output is obtained from a standard single-mode fiber (Corning SMF-28). Consequently, the beam is truly diffraction limited, which was independently proven by M^2 measurements. Further increase of peak power is limited by onset of significant spectral broadening due to nonlinear effects, primarily four-wave mixing. Numerical simulations based on six-level rate equations with full position- and time-dependence were developed to model propagation of pulses through the amplifier chain. This capability allows minimization of the amplified spontaneous emission, which can be directly measured using a fast acousto-optic modulator to gate the pulses.

OCIS codes: (140.3510) Lasers, fiber; (060.2320) Fiber optics amplifiers and oscillators.
http://dx.doi.org/10.1364/OL.39.002695

In the last decade, fiber laser development has focused on Yb-fiber lasers because of their excellent capacity for high-power operation [1,2]. However, there are various established and emerging applications that require the relative eye safety afforded by longer wavelength Er-fiber lasers. These applications include remote laser sensing [3] and lidars [4], and require low-cost, mechanically robust, high-energy pulsed laser sources with average power and repetition rates higher than reported so far, while maintaining excellent beam quality. Achievement of high peak powers is limited by the well-known difficulties arising from the strong nonlinear effects of confining beam propagation over several meters in the small core of a single-mode fiber (SMF). In addition to four-wave-mixing, stimulated Raman scattering [5] and for narrow line-width lasers, stimulated Brillouin scattering [5] are the dominant effects, resulting in spectral broadening and in the extreme, destabilization of the laser operation or even damaging the components of the laser system.

The standard approach to reach high peak power is to reduce the nonlinear effects by using large-mode area fibers [6–8]. Increasing the core diameter of the gain fiber requires elaborate methods of higher-order mode suppression, which does not always succeed. For certain applications, however, the beam quality should be truly diffraction-limited, devoid of any higher-order modes. A guaranteed way to ensure pure single-mode operation is to use standard SMF, such as SMF-28 [9].

In that case, the gain fiber length must be minimized to limit the nonlinear effects. Compared to Yb-doped fibers, Er-doped fibers have relatively low pump absorption levels, requiring long fiber lengths and resulting in enhanced nonlinear effects. This appears to be a primary reason behind the relatively poor peak-power performance of pulsed Er-fiber lasers compared to Yb-fiber lasers. Partial relief comes from tandem pumping [10], which allows shortening of the required gain fiber, reducing nonlinear effects indirectly. Codoping with Yb ions addresses the issue of low pump absorption, also allowing for shorter gain lengths, but introduces a stronger spontaneous amplified emission (ASE) problem. A significant amount of ASE can be generated in the gain fiber even at a relatively high repetition rate [11]. Recently, 200 μJ, 200 ns pulses with a low repetition rate (Hz range) were demonstrated with 17 μm core diameter gain fiber by using pulsed pump source, which allows suppression of ASE content at such low repetition rate [12].

Accurate characterization of the ASE content in the time domain is crucial since several publications are reporting Er-fiber and Er–Yb-fiber systems at very low repetition rates. We attribute these reports to inferral of the ASE content purely by analysis of the optical spectrum. This method inherently assumes that all ASE is broadband, which is not necessarily true. In a multistage system, particularly with spectral filters between the stages, ASE can start to build up within a narrow spectral region matching that of the signal, becoming difficult to distinguish from the signal. Direct time-domain characterization can help avoid this pitfall.

Here, we report on an all-fiber-integrated, master-oscillator power-amplifier (MOPA) system, where the power amplifier is based on Er–Yb-codoped double-clad (DC) fiber. The system produces more than 10 W of average output power at 100 kHz repetition rate with ~5 ns pulse duration and 100 μJ of pulse energy. We proposed and used a time-domain method to characterize the ASE content. We used narrowband filters to suppress ASE by the use of narrow-band filters, time-gating using an acousto-optic modulator (AOM) as well as careful optimization of the number of amplifier stages and the repetition rate. This optimization is made possible by using an accurate numerical model, which, in addition to helping us reduce the ASE, allows effective use of gain depletion to achieve sub-5-ns pulses, starting from a seed source of 15 ns.

We have developed a numerical model to describe propagation and amplification of pulses in the multistage

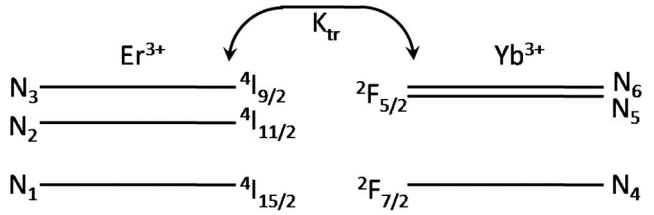

Fig. 1. Schematic of energy levels for the Er–Yb codoped fiber.

amplifier. The model is based on numerically solving time- and space-dependent rate equations for Er-doped fiber (three-level system) and Er–Yb-codoped fiber (six-level system) [13,14]. The simplified rate equations are given below and Fig. 1 depicts the corresponding energy diagram for the Er–Yb-codoped fiber:

$$\dot{N}_6 = W_{46}^{(p)}(N_4 - N_6) - \sigma_{65}N_6 - K_{\mathrm{tr}}(N_6N_1 - N_3N_4), \quad (1)$$

$$\dot{N}_5 = \sigma_{65}N_6 - W_{54}^{(s)}N_5 + W_{45}^{(s)}N_4 - \sigma_{54}N_5 - K_{\mathrm{tr}}(N_5N_1 - N_3N_4), \quad (2)$$

$$\dot{N}_3 = W_{13}^{(p)}(N_1 - N_3) + K_{\mathrm{tr}}(N_6N_1 - N_3N_4) - \sigma_{32}N_3 + K_{\mathrm{tr}}(N_5N_1 - N_3N_4), \quad (3)$$

$$\dot{N}_2 = \sigma_{32}N_3 - W_{21}^{(s)}N_2 + W_{12}^{(s)}N_1 - \sigma_{21}N_2, \quad (4)$$

$$N_{\mathrm{Er}} = N_1 + N_2 + N_3, \quad (5)$$

$$N_{\mathrm{Yb}} = N_4 + N_5 + N_6. \quad (6)$$

Here, $\dot{N}_i$ denotes the time derivative of N_i, which is the number of ions in ith state, where $i = 1, \ldots, 6$. The equation

$$W_{ij}^{(p,s)} = \frac{P^{(p,s)}}{h\nu^{(p,s)}A_{\mathrm{eff}}}\delta_{ij} \quad (7)$$

shows the probabilities for absorption and stimulated emission transition from level i to level j, for pump and signal, where $P^{(p,s)}$ are the corresponding pump or signal power, and $h\nu^{(p,s)}$ are the pump or signal photon energy, respectively. A_{eff} is the effective core area, δ_{ij} are the stimulated emission/absorption transition cross-sections from level i to level j, and σ_{ij} are the probabilities of spontaneous transitions (radiative and nonradiative) from level i to level j. K_{tr} is the energy transfer coefficient between the Er and the Yb levels. These coupled equations are solved using finite differences method. This way, time- and space-resolved dynamics are considered, allowing us to account for processes such as dynamic gain saturation, which results in temporal reshaping of the pulse and time-dependent ASE creation. For the Er-only amplifier stages, the same model is used after simply eliminating the Yb levels and using the corresponding parameters.

Figure 2 shows simplified schematics of the experimental setup. The number of amplifier stages, the relative gain factors achieved by them, the placement of the bandpass filters and the placement of the AOM have

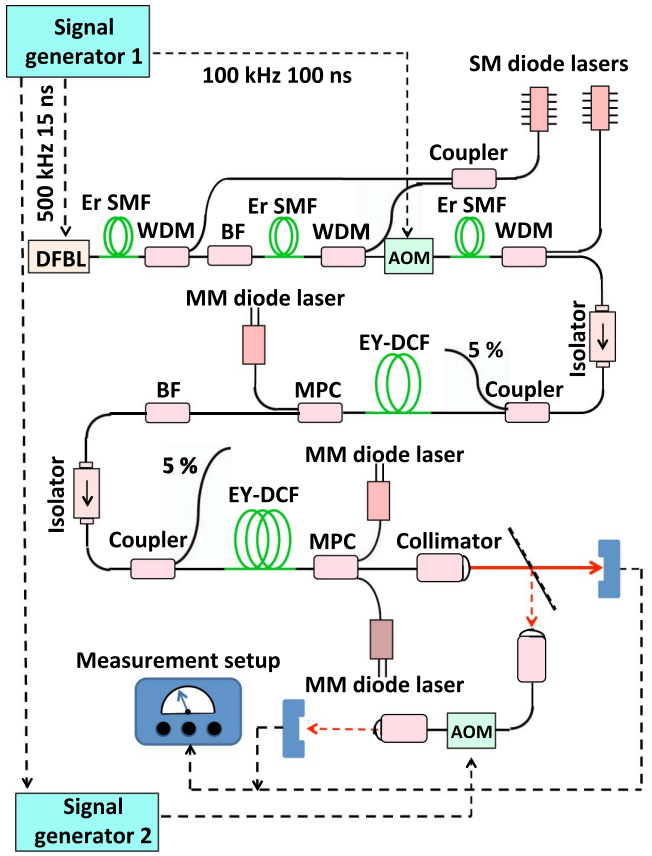

Fig. 2. Schematic of the experiment setup. BF, bandpass filter; MM, multimode; SM, single-mode; MPC, multiple-port pump-signal combiner; WDM, wavelength division multiplexer; AOM, acousto-optic modulator; and DBFL, distributed feedback laser.

all been optimized using the numerical simulations and through careful experimental characterization in an iterative procedure, culminating in the current design. As seed source, we use an electronically modulated distributed feedback semiconductor laser (DFBL).

The current supplied to the DFBL is modulated electronically to produce pulses of adjustable duration and as short as 15 ns. Since the DFBL is limited in the current it can handle, the maximum pulse energy is limited to about 1.5 nJ for this pulse duration. Thus, we operate it at 500 kHz, corresponding to 0.2 mW, to be able to saturate the first preamplifier that follows. The seed signal is amplified in two preamplifiers, first in a 6.5 μm mode field diameter (MFD), 40-cm-long Er-fiber with absorption level of 80 dB/m at 1530 nm to 9 mW (18 nJ) and then in a 6.5 μm MFD, 120-cm-long Er-fiber with absorption level of 80 dB/m at 1530 nm to 120 mW.

These two stages are pumped in core by a single pump diode (operating at 976 nm), the output of which is split to deliver 80 and 400 mW to the first and second preamplifiers, respectively. ASE generation is kept in check with a bandpass filter of 100 GHz bandwidth. The pulses then traverse a fiber-coupled AOM, where the pulse train is gated with square pulses of temporal width of 100 ns to reduce the repetition rate (to the range of 50–100 kHz). In addition to lowering the repetition rate, the gating operation (with a suppression coefficient of >50 dB) blocks any ASE between the pulses.

Due to the 50% insertion loss of the AOM, there are three additional amplifier stages. The first stage consists of a 1.2 m Er-doped SMF (6.5 μm MFD, core absorption of 80 dB/m at 1530 nm), which also is core-pumped by a similar single-mode pump diode, amplifying the signal to 169 mW. The second stage is comprised of a 3 m DC Er–Yb-codoped fiber with 10 μm core and 125 μm cladding diameter (Coractive Inc.). The pump source is a multimode diode at 976 nm coupled to a 105 μm fiber, the output of which is delivered through a signal-pump combiner (MPC) into the cladding region in the backward direction. A bandpass filter and an isolator follow, to reduce ASE and limit nonlinear spectral broadening, and to protect the amplifier from backward-propagating light from the final amplifier stage, respectively. The average signal power at this point reaches 1.2 W. The final power amplifier stage is comprised of a 5.5-m-long DC Er–Yb-codoped fiber with 12 μm core and 130 μm cladding diameter (Coractive Inc.), which also is backward pumped in the cladding by two high-power fiber-coupled multimode diodes at 976 nm through a MPC. Both second and third stages MPCs were commercially available (Lightcomm Technology) with 15 W of power handling for each pump port.

We did not apply any special precautions to ensure pump diodes from possible signal leakage to the pump ports. A fiber-pigtailed collimator, capable of handling high powers, is spliced to the signal port of MPC. The final average output power reaches 10 W [Fig. 3(a)]. The fiber of the signal port of the combiner and that of the output collimator are both SMF-28, which is strictly single-mode at 1.55 μm and thus produces a near diffraction-limited, spatially Gaussian output beam of measured $M^2 = 1.04$ [Fig. 3(b)]. We stress that, although the final amplifier fiber can in principle support multiple transverse modes (V 4.6), we observed no appreciable power loss coupling its output into the SMF-28 output pigtail. This shows that the optical power exiting the fiber amplifier is predominantly confined within the fundamental LP01 mode.

For direct, time-domain characterization of the ASE content of the amplifier signal, a small part of the output signal can be channelled into a fiber-coupled AOM. If the AOM is gated with a negative ~100 ns square pulse, synchronized to the pulse train, this operation drops only the pulse, revealing any ASE signal that has accumulated between the pulses. In this configuration, measurement of the ratio of the transmitted power with the pulse dropped to the power with AOM passing all the signal gives the fraction of optical energy between the pulses (i.e., the ratio of ASE to the total signal). We consider this to be a more reliable method to assess ASE content that spectral measurements and the use of energy meters, which also can be misleading since the ASE signal is not a strictly continuous wave [Fig. 4(a)] due to its time-dependent buildup.

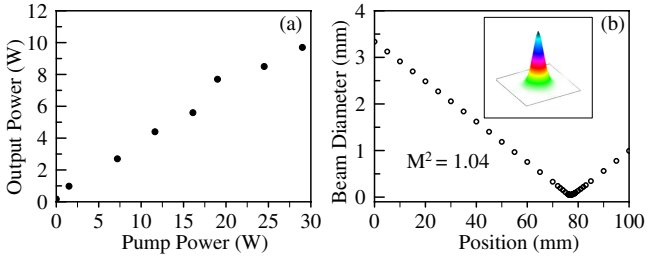

Fig. 3. (a) Measured signal output power as a function of pump power for final stage amplifier. (b) Dependence of beam diameter at the 1/e-level on position, along with fitted M^2 value. Inset: far-field 3D beam profile.

Theoretical calculations and experimental measurements demonstrate that operation of the laser system at repetition rates below 100 kHz results in steep increases of ASE (Fig. 4). Even with long pulses and low peak powers, which result in negligible spectral broadening, the presence of substantial amounts of ASE is not readily discernible from the optical spectrum, which remains narrow due to the use of the bandpass filters. However, depending on the experimental conditions, the AOM-based measurement reveals that the amount of ASE varies between 60% and 80% of the total output power at 50 kHz.

Although it is impossible to time-resolve the ASE signal due to the small duty cycle and limited amplitude resolution (limited by 8-bit digitization) of an oscilloscope directly, it is possible to qualitatively visualize the ASE build-up dynamics by strongly oversaturating a photodetector, such that the gradual ASE buildup between the pulses is resolved [Fig. 4(a)]. We observe that ASE starts to grow substantially about 10 μs after each pulse. This suggests that the repetition rate for our amplifier configuration should be around 100 kHz to limit ASE to between 2% and 4%. These experimental observations are consistent with earlier investigations of ASE creation [11], where 17 μm core gain fiber was used. Furthermore, our numerical simulations are in good agreement with the measurements [Fig. 4(b)].

Figure 5 presents the operational characteristics of the system at 100 kHz. Amplified pulses of ~5 ns duration can routinely be obtained, corresponding to peak power as much as 20 kW at 10 W average power and 100 kHz. Due to the high peak power, we observed significant spectral broadening after the last stage (Fig. 5(a)). However, as confirmed by the direct ASE measurements, the ASE level is kept very low.

Due to dynamic gain saturation, the final pulse width depends sensitively on the frontal slope of the seed pulse, which can be used as a control parameter to tune the final pulse width. The pulse duration decreases significantly starting from 15 ns to less than 4 ns, but

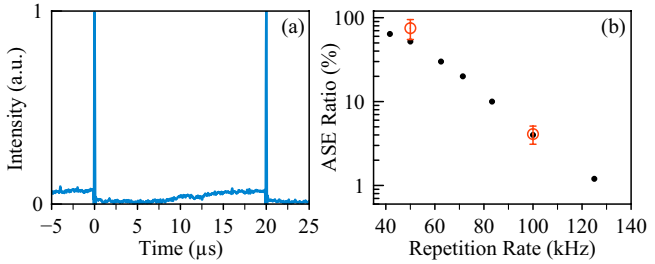

Fig. 4. (a) Temporal profile of the amplified pulse train showing the ASE buildup at 50 kHz, where the vertical axis is not a linear function of power due to extreme saturation of the photodetector to render the ASE signal visible. (b) Variation of the ASE ratio in the amplified signal as a function of repetition rate. Simulation and experimental results are represented by full and empty circles, respectively.

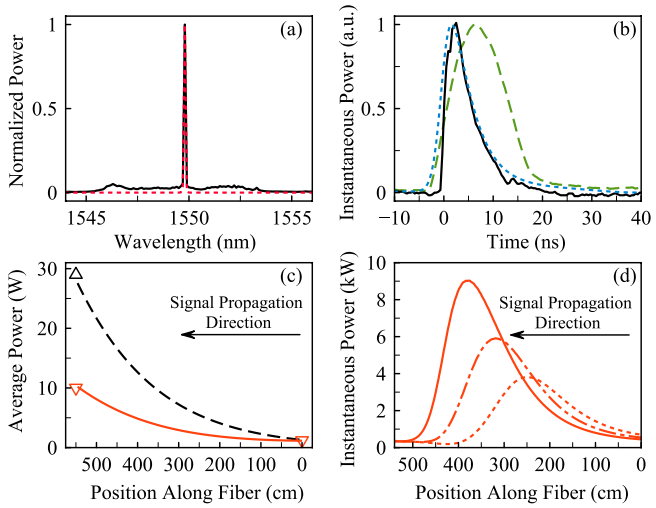

Fig. 5. (a) Measured optical spectra of the seed (dotted line) and amplified pulses at full power (solid line). (b) Temporal profiles of the pulses: Seed pulse generated by the DFBL (dashed line), simulated (dotted line) and experimentally measured (solid line) amplified pulses at full power. (c) Evolution of the average signal (solid line) and pump (dashed line) power along the final-stage fiber amplifier obtained from simulations. Measured signal (downward triangles) and pump (upward triangle) power show the good agreement between simulations and experiments. (d) Simulated evolution of the pulse as it propagates inside of the final-stage amplifier, showing the steepening of the leading edge due to gain depletion.

we typically obtain 5 ns [Fig. 4(b)]. The buildup of average power in the final stage of amplification is accurately described by simulations, when compared to experiments [Fig. 5(c)]. The evolution of the temporal shape of the pulse within the amplifier illustrates the well-known mechanism of pulse shortening [Fig. 5(d)].

In conclusion, guided by a detailed, accurate numerical model and through careful experimental characterization, we have developed a truly single-mode laser source producing 10 W, 5 ns, 100 kHz pulses at the eye-safe wavelength of 1.55 μm. The laser beam is always confined in fiber or a fiberized component at all points, rendering the system immune to mechanical perturbations.

To the best of our knowledge, this is the highest pulse energy reported for strictly single-mode operation at this wavelength. Theoretical and experimental optimization suggest that operation at repetition rates below 100 kHz would require pulsed pumping to keep ASE levels below 10% when Er–Yb-codoped fiber is used. A detailed theoretical analysis of the ASE generation process and the ultimate limits to its minimization will be covered in a future publication. We expect this robust, high-power, diffraction-limited, yet compact and all-fiber laser system to find various applications, particularly in remote sensing and lidars.

This work was supported by the SANTEZ Project No. 00255.STZ.2008-1 and by the SSM “Fiber Laser” Project.

References

1. D. J. Richardson, J. Nilsson, and W. A. Clarkson, J. Opt. Soc. Am. B **27**, B63 (2010).
2. C. Jauregui, J. Limpert, and A. Tünnermann, Nat. Photonics **7**, 861 (2013).
3. S. Gupta, D. Engin, K. Puffenberger, S. Litvinovich, F. Kimpel, and R. Utano, Proc. SPIE **8876**, 88760E (2013).
4. J. Lee, Y.-J. Kim, K. Lee, S. Lee, and S.-W. Kim, Nat. Photonics **4**, 716 (2010).
5. G. Agrawal, *Nonlinear Fiber Optics* (Academic, 2006).
6. V. Philippov, C. Codemard, Y. Jeong, C. Alegria, J. K. Sahu, J. Nilsson, and G. N. Pearson, Opt. Lett. **29**, 2590 (2004).
7. C. Codemard, C. Farrel, P. Dupriez, V. Philippov, J. K. Sahu, and J. Nilson, C.R. Physique **7**, 170 (2006).
8. E. Petersen, W. Shi, A. Chavez-Pirson, and N. Peyghambarian, Appl. Opt. **51**, 531 (2012).
9. I. Pavlov, E. Ilbey, E. Dulgergil, A. Bayri, and F. O. Ilday, Opt. Express **20**, 9471 (2012).
10. E. Lim, S. Alam, and D. J. Richardson, Opt. Express **20**, 18803 (2012).
11. F. Di Teodoro, M. Savage-Leuchs, and M. Norsen, Electron. Lett. **40**, 1525 (2004).
12. P. Wan, J. Liu, L.-M. Yang, and F. Amzajerdian, Opt. Express **19**, 18067 (2011).
13. B. Morasse, S. Agger, C. Hovington, S. Chatigny, E. Gagnon, J.-P. de Sandro, and C. Poulsen, Proc. SPIE **6453**, 645324 (2007).
14. M. Karasek, IEEE J. Quantum Electron. **33**, 1699 (1997).